Anal. Chem. **2008,** *80,* 7363–7371

Depth Resolution During C_{60}^+ Profiling of Multilayer Molecular Films

Leiliang Zheng,[†] Andreas Wucher,[‡] and Nicholas Winograd*[,†]

Department of Chemistry, The Pennsylvania State University, 104 Chemistry Building, University Park, Pennsylvania 16802, and Physics Department, University of Duisburg—Essen, Duisburg, 47048 Germany

Time-of-flight secondary ion mass spectrometry is utilized to characterize the response of Langmuir−Blodgett (LB) multilayers under the bombardment by buckminsterfullerene primary ions. The LB multilayers are formed by barium arachidate and barium dimyristoyl phosphatidate on a Si substrate. The unique sputtering properties of the C_{60} ion beam result in successful molecular depth profiling of both the single component and multilayers of alternating chemical composition. At cryogenic (liquid nitrogen) temperatures, the high mass signals of both molecules remain stable under sputtering, while at room temperature, they gradually decrease with primary ion dose. The low temperature also leads to a higher average sputter yield of molecules. Depth resolution varies from 20 to 50 nm and can be reduced further by lowering the primary ion energy or by using glancing angles of incidence of the primary ion beam.

The development of polyatomic projectiles for cluster-based secondary ion mass spectrometry (SIMS) is opening new opportunities for materials characterization. Of special interest is the emergence of molecular depth profiling whereby the projectile removes molecules in nearly a layer-by-layer fashion without the accumulation of chemical damage.[1−7] This problem has plagued atomic projectiles for many years[8] and has limited sensitivity. When the molecular samples are bombarded with cluster ion sources, the energy is deposited close to the surface and the chemical damage is then removed as fast as it accumulates, leaving subsurface layers relatively intact.[9−15] The quality of the depth profile has recently been characterized by a cleanup efficiency parameter derived from a simple erosion model for molecular solids.[16] Among all the cluster projectiles, buckminsterfullerene (C_{60}^+) generally exhibits the highest cleanup efficiency.[17,18]

New fundamental studies of the sputtering process are now required to optimize the experimental parameters for molecular depth profiling. The literature concerning the interactions between energetic cluster ions and molecular solids has grown rapidly, including experimental approaches[16,19−26] and molecular dynamic (MD) simulations.[11−13,27−29] While MD simulations have provided insightful understanding, much of the experimental work lacks a quantitative understanding for comparison to the simulation results. Moreover, most of the molecular depth profiling experiments are performed on organic systems either with uniform chemical content or with unknown composition.[3,4,30,31] The analysis of buried organic layers under cluster bombardment has been shown to be feasible, but the degree of beam-induced mixing between organic layers is not fully understood. This information is important to cluster SIMS applications in biology since biomaterials are generally chemically heterogeneous and complex. Hence, it is essential to quantify the organic−organic interface

* To whom correspondence should be addressed. E-mail: nxw@psu.edu.
[†] The Pennsylvania State University.
[‡] University of Duisburg-Essen.

(1) Gillen, G.; Roberson, S. *Rapid Commun. Mass Spectrom.* **1998**, *12*, 1303–12.
(2) Mahoney, C. M.; Roberson, S. V.; Gillen, G. *Anal. Chem.* **2004**, *76*, 3199–207.
(3) Cheng, J.; Winograd, N. *Anal. Chem.* **2005**, *77*, 3651–9.
(4) Sostarecz, A. G.; McQuaw, C. M.; Wucher, A.; Winograd, N. *Anal. Chem.* **2004**, *76*, 6651–8.
(5) Sostarecz, A. G.; Sun, S.; Szakal, C.; Wucher, A.; Winograd, N. *Appl. Surf. Sci.* **2004**, *231−2*, 179–82.
(6) Wucher, A.; Sun, S. X.; Szakal, C.; Winograd, N. *Anal. Chem.* **2004**, *76*, 7234–42.
(7) Wagner, M. S. *Anal. Chem.* **2005**, *77*, 911–22.
(8) Winograd, N. *Anal. Chem.* **2005**, *77*, 142A–9A.
(9) Postawa, Z.; Czerwinski, B.; Szewczyk, M.; Smiley, E. J.; Winograd, N.; Garrison, B. J. *Anal. Chem.* **2003**, *75*, 4402–7.
(10) Postawa, Z.; Czerwinski, B.; Szewczyk, M.; Smiley, E. J.; Winograd, N.; Garrison, B. J. *J. Phys. Chem. B* **2004**, *108*, 7831–8.
(11) Postawa, Z.; Czerwinski, B.; Winograd, N.; Garrison, B. J. *J. Phys. Chem. B* **2005**, *109*, 11973–9.
(12) Garrison, B. J.; Ryan, K. E.; Russo, M. F.; Smiley, E. J.; Postawa, Z. *J. Phys. Chem. C* **2007**, *111*, 10135–7.
(13) Russo, M. F.; Garrison, B. J. *Anal. Chem.* **2006**, *78*, 7206–10.
(14) Aoki, T.; Matsuo, J. *Nucl. Instrum. Methods B* **2004**, *216*, 185–90.
(15) Seki, T.; Matsuo, J. *Nucl. Instrum. Methods B* **2004**, *216*, 191–5.
(16) Cheng, J.; Wucher, A.; Winograd, N. *J. Phys. Chem. B* **2006**, *110*, 8329–36.
(17) Cheng, J.; Kozole, J.; Hengstebeck, R.; Winograd, N. *J. Am. Soc. Mass Spectrom.* **2007**, *18*, 406–12.
(18) Szakal, C.; Kozole, J.; Russo, M. F.; Garrison, B. J.; Winograd, N., *Phys. Rev. Lett.* **2006**, 96.
(19) Cheng, J.; Winograd, N. *Appl. Surf. Sci.* **2006**, *252*, 6498–501.
(20) Gillen, G.; Batteas, J.; Michaels, C. A.; Chi, P.; Small, J.; Windsor, E.; Fahey, A.; Verkouteren, J.; Kim, K. J. *Appl. Surf. Sci.* **2006**, *252*, 6521–5.
(21) Kozole, J.; Wucher, A.; Winograd, N. *Anal. Chem.* **2008**, *80*, 5293−5301.
(22) Mahoney, C.; Fahey, A.; Gillen, G. *Anal. Chem.* **2007**, *79*, 828–36.
(23) Mahoney, C.; Fahey, A.; Gillen, G.; Xu, C.; Batteas, J. *Anal. Chem.* **2007**, *79*, 837–45.
(24) Shard, A. G.; Green, F. M.; Brewer, P. J.; Seah, M. P.; Gilmore, I. S. *J. Phys. Chem. B* **2008**, *112*, 2596–605.
(25) Shard, A. G.; Brewer, P. J.; Green, F. M.; Gilmore, I. S. *Surf. Interface Anal.* **2007**, *39*, 294–8.
(26) Wagner, M. S. *Anal. Chem.* **2004**, *76*, 1264–72.
(27) Delcorte, A.; Garrison, B. J. *J. Phys. Chem. C* **2007**, *111*, 15312–24.
(28) Russo, M. F.; Szakal, C.; Kozole, J.; Winograd, N.; Garrison, B. J. *Anal. Chem.* **2007**, *79*, 4493–8.
(29) Smiley, E. J.; Winograd, N.; Garrison, B. J. *Anal. Chem.* **2007**, *79*, 494–9.
(30) Fletcher, J. S.; Lockyer, N. P.; Vaidyanathan, S.; Vickerman, J. C. *Anal. Chem.* **2007**, *79*, 2199–206.
(31) Jones, E. A.; Lockyer, N. P.; Vickerman, J. C. *Anal. Chem.* **2008**, *80*, 2125–32.

10.1021/ac801056f CCC: $40.75
Published on Web 09/06/2008

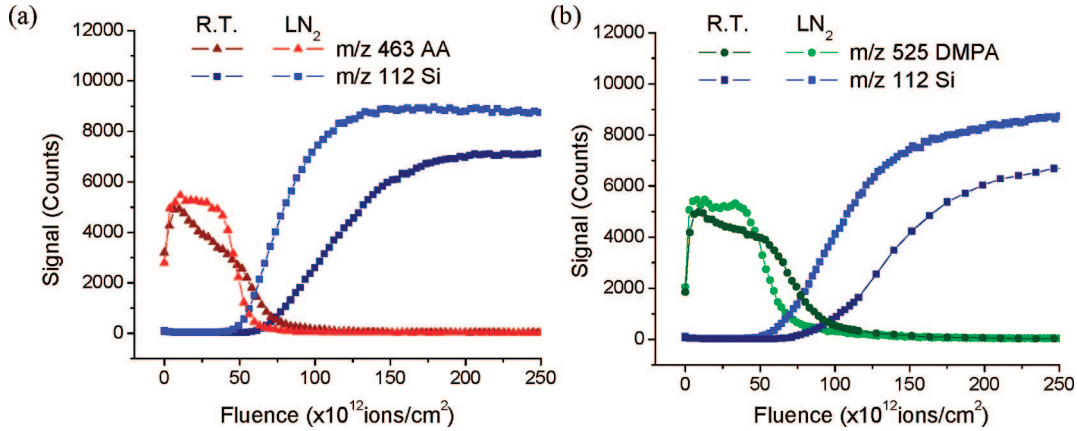

Figure 1. Depth profiles of single-component LB films of (a) 105-nm AA and (b) 96-nm DMPA deposited on piranha-etched silicon substrates. Sputter erosion and data acquisition were performed using 40-keV C_{60}^+ projectiles. Profiles measured at RT are denoted by dark red, green, and blue lines, and the bright red, green, a d blue lines represent profiles measured at LN_2 temperature. Note that *m*/*z* 463 was not observed in the DMPA spectrum and *m*/*z* 525 was observed in the AA spectrum.

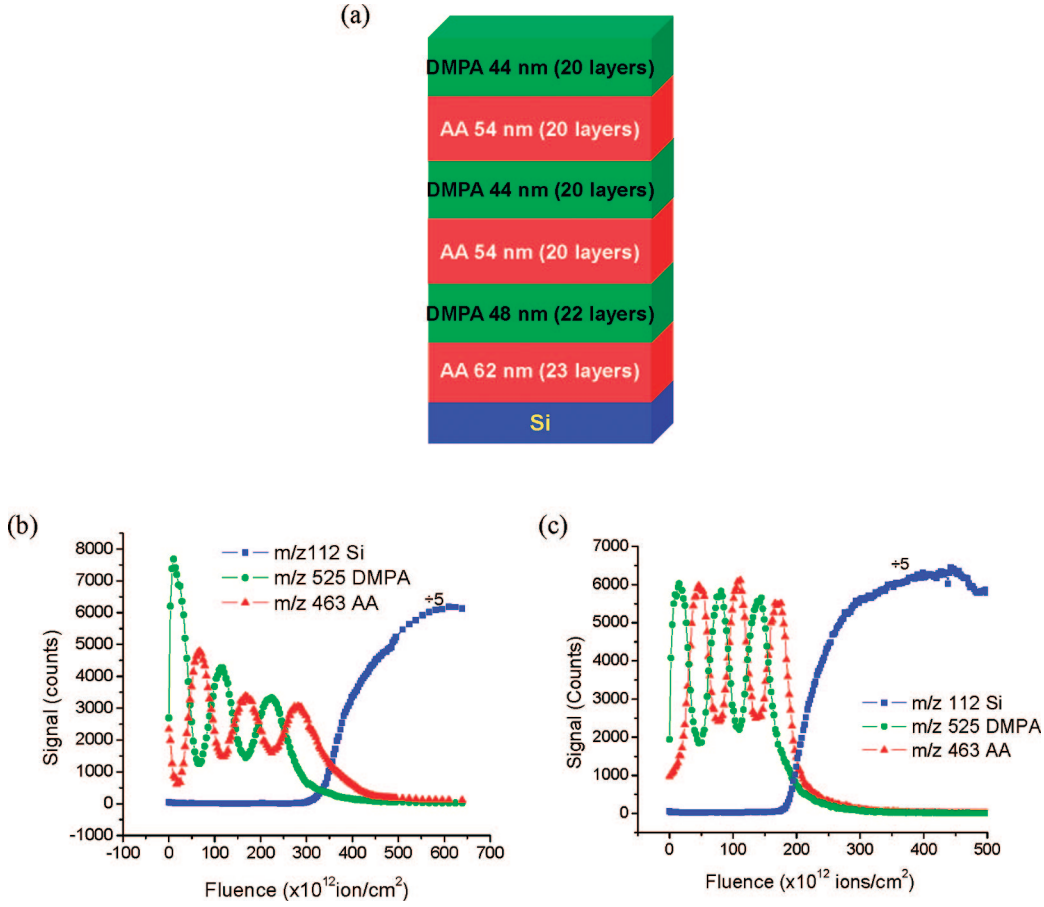

Figure 2. (a) Chemical structure of the alternating LB film of AA and DMPA deposited on piranha-etched silicon substrate and the depth profiles measured at (b) room temperature and (c) liquid nitrogen temperature using 40-keV C_{60}^+ projectiles.

width during molecular depth profiling to determine the optimum parameters that lead to the highest information content.

A robust and reproducible model system with well-defined chemical structures is a first step in obtaining quantitative information about buried interfaces using cluster ion bombardment. Previously, we have utilized trehalose sugar films spin-cast on Si substrates to develop an erosion model that uses the damage cross section, the altered layer thickness at the surface, and the sputtering yield as parameters.[3,16] A different system consisting of organic δ layers built by a large tetrahedral molecule, Irganox, has also been reported.[25] Results using this system have shown that the interface width is larger than the δ layer thickness (2.5 nm) and is limited mainly by the development of surface topography. In early studies, Langmuir−Blodgett (LB) films were analyzed by static SIMS to quantify sampling depth in organic materials.[32,33] Recently, we also reported on using LB techniques

(32) Johnson, R. W.; Cornelio-Clark, P. A.; Gardella, J. A. **1992**, 113–21.

Table 1. Sputter Yields (Molecule Equivalents/C_{60}^+) of DMPA and AA[a]

		single-component film	Alternating film		
			top block	middle block	bottom block
AA	room temperature	329 ± 15	294	248	207
	low temperature	448 ± 18	421	408	427
DMPA	room temperature	123 ± 7	133	107	94
	low temperature	166 ± 9	159	164	168

[a] The data of single-component film represent averages of at least 3 parallel experiments of samples with the same chemical structure.

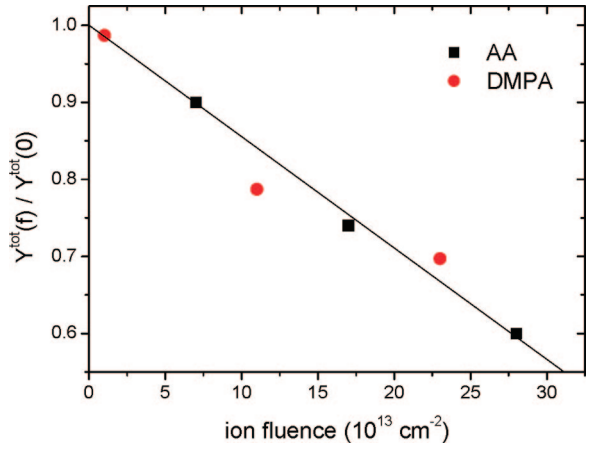

Figure 3. Total sputter yield vs primary ion fluence during depth profiling through alternating LB multilayer film. The data were normalized to the value at the beginning of the depth profile.

Table 2. Surface Roughness (nm) (Roughness Average Ra with the Field of View of 20 μm × 20 μm) of Si Substrate and Resulting LB Films[a]

	Si	LB film before sputtering	LB films after 15-s sputtering at 400 × 400 μm
methanol clean	1.1 ± 0.2	9.5 ± 1	8.7 ± 1
ozone clean	2.7 ± 0.8	13 ± 2	12 ± 2
piranha each	4.8 ± 1	16 ± 2	15 ± 2

[a] The data are based on at least 3 parallel measurements.

to form chemically alternating organic thin films as a molecular depth profiling model to study organic−organic interfaces.[34] Multilayer LB films have been well-characterized and are known to form sharp boundaries between the layers. The preliminary study showed that chemical structures were accurately represented by the profile of molecule-specific ion signals and that depth resolution can be calculated by a simple curve-fitting approach.[34] No evidence for topography formation was noted during the erosion process.

Using chemically alternating LB multilayers as a model, here we investigate the experimental parameters necessary for optimization of molecular depth profiling, particularly so that optimum depth resolution can be achieved. The system consists of alternating barium arachidate (AA) and barium dimyristoyl phosphatidate (DMPA) layers ~50 nm thick that is depth profiled by a C_{60}^+ ion beam. Various parameters that potentially affect the depth profile results are studied, including experimental temperature, sample roughness, primary ion energy, and incident angle. Our results show that chemical damage accumulation is minimized when the sample is maintained at liquid nitrogen temperature. Samples with slightly different topography yield similar depth resolution, implying that this property is not largely affected by surface roughness. The parameters of the primary ion beam also have large effects on the profile quality. For example, the highest depth resolution is achieved at glancing incident angles, but the observed interface widths increase slightly with increasing kinetic energy. In general, this model system provides a platform for determining the condition for optimum depth resolution and for elucidating fundamental aspects of the interaction of energetic cluster ion beams with molecular solids.

EXPERIMENTAL SECTION

Materials. Arachidic acid, barium chloride (99.999%), potassium hydrogen carbonate (99.7%), copper(II) chloride (99.999%), and all solvents were purchased from Sigma-Aldrich (Allentown, PA). The DMPA was purchased from Avanti Polar Lipids (Alabaster, AL). All chemicals were used without further purification. Water used in preparation of all LB films was obtained from a Nanopure Diamond Life Science Ultrapure Water System (Barnstead International, Dubuque, IA) and had a resistivity of at least 18.2 MΩ·cm.

Substrates and Film Preparations. A 3 × 3-in. single-crystal (100) silicon wafer was used as the substrate for all LB films. The substrates were treated by three types of cleaning methods before LB film application. The substrate was either sonicated in methanol for 10 min, treated with ozone for 10 min, or cleaned by piranha etch (3:1 H_2SO_4/H_2O_2). *(Extreme caution must be exercised when using piranha etch. An explosion-proof hood should be used.)* After cleaning, the substrates were rinsed with high-purity water several times to ensure hydrophilicity of the Si/SiO_2 surface. A drop of pure water was placed onto the substrate before film application. The drop spread on the surface, indicating the hydrophilicity of the substrate. A Kibron μTrough S-LB (Helsinki, Finland) was used for isotherm acquisition and multilayer LB film preparation. Details of the LB film formation have been described previously.[34] The value of the area/molecule during film transfer is used to calculate the film density needed for sputter yield calculations. At least three layers of AA were initially applied onto the substrate at first to ensure orderly multilayer formation. Subsequently, an even number of DMPA or AA layers were deposited consecutively. At least 15 min was allowed to elapse between subsequent deposition cycles to ensure complete drying of the substrate.

Instrumentation. A previously described TOF-SIMS instrument was employed for all experiments.[35] Depth profiling of the LB films was performed by a 40-keV C_{60} ion source (IOG 40-60, Ionoptika; Southampton, U.K.), which is directed to the target

(33) Johnson, R. W.; Cornelio-Clark, P. A.; Li, J.-X.; Gardella, J. A., *Secondary Ion Mass Spectrometry VIII*; Wiley: New York, 1992; pp 293−6.
(34) Zheng, L.; Wucher, A.; Winograd, N. *J. Am. Soc. Mass Spectrom.* **2007**, *19*, 96–102.
(35) Braun, R. M.; Blenkinsopp, P.; Mullock, S. J.; Corlett, C.; Willey, K. F.; Vickerman, J. C.; Winograd, N. *Rapid Commun. Mass Spectrom.* **1998**, *12*, 1246–52.

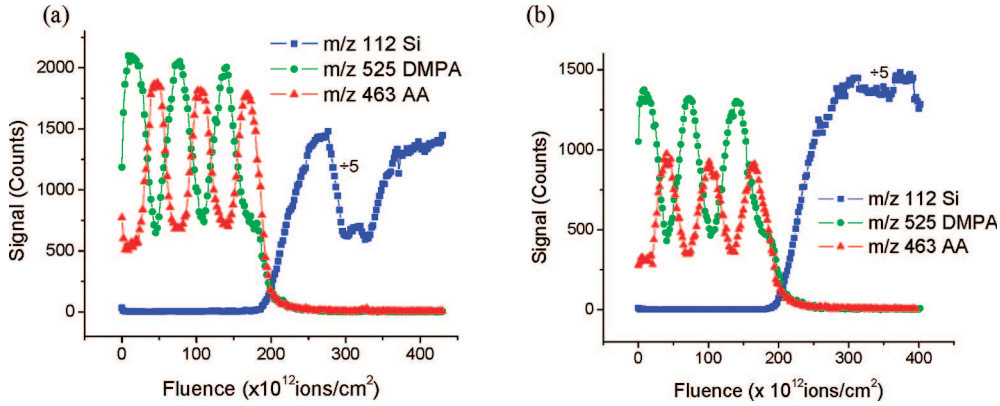

Figure 4. Depth profiles of alternating LB film of AA and DMPA deposited on silicon substrate cleaned with (a) ozone treatment and (b) methanol sonication measured at liquid nitrogen temperature using 40-keV C_{60}^+ projectile ions.

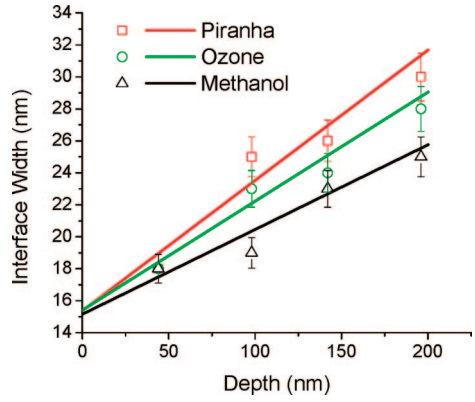

Figure 5. Interface width vs eroded depth for alternating LB films with different initial surface roughness. Straight lines: linear least-squares fit for each film. Error bars correspond to ±5% of the calculated value.

surface at an angle of 40° relative to the surface normal. The kinetic energy of the primary ions was adjusted by varying the anode voltage between 20 and 40 kV or by selecting the charge state of the primary ions by means of a Wien filter. The mass spectrometer was operated in a delayed extraction mode with 50-ns delay time between the primary ion pulse and the secondary ion extraction pulse. Charge compensation was found to be unnecessary for the positive ion SIMS mode. Secondary ion intensities were calculated by integrating the respective mass peak in the TOF spectrum. A mass resolution of ~2500 was routinely achieved at the mass of the molecule-specific peak of DMPA at m/z 525. The incident angle of the projectile ion beam was altered by tilting the sample surface relative to the stage. Although this procedure prevents comparison of ion yields at different angles since the angle between the surface normal and the ion optical axis of the mass spectrometer also changes, ion yields acquired during a depth profile are comparable since the angle is kept constant during the data acquisition.

A depth profile was performed by alternating between mass spectral data acquisition and sputter erosion cycles. During an erosion cycle, the films were bombarded with the projectile ion beam operated in dc mode and rastered across a surface area ("field of view") of dimensions $\Delta x \cdot \Delta y$ with $\Delta y = \Delta x/\cos\theta$ and Δx ranging from 300 to 600 μm. (The angle θ is the impact angle of the primary beam with respect to the surface normal). A digital raster scheme with 256 × 256 pixels was employed, thus rendering a pixel step size between 1.2 and 2.4 μm, a value that is small compared to the probe size of the projectile beam (~30 μm). The total bombardment time during each erosion cycle varied from 3 to 10 s, resulting in a total dwell time between 50 and 150 μs on each pixel. In order to minimize redeposition effects and ensure a uniform erosion rate, several frame scans were made during each erosion cycle, limiting the pixel dwell time in each individual frame to 10 μs. Between erosion cycles, SIMS spectra were taken from the center of the sputtered region, with the ion beam operated in pulsed mode (pulse duration ~50 ns) and rastered across a quarter of the erosion area. The total projectile ion fluence applied during each acquisition cycle was kept below 10^{11} cm^{-2}, ensuring negligible erosion even when accumulated over hundreds of data points in the depth profile.

Ellipsometry and Atomic Force Microscopy (AFM) Measurement. AFM (Nanopics 2100, KLA-Tencor, San Jose, CA) was used to measure the surface roughness and the sputter crater depth. The maximum field of view of 800 μm × 800 μm in contact mode allows a convenient one-step measurement of the entire sputter crater. The thickness of the LB monolayers was determined by a single-wavelength (632.8 nm, 1-mm spot size, 70° angle of incidence) Stokes ellipsometer (Gaertner Scientific Corp., Skokie, IL; model LSE). The thickness of the LB films was found to be equal to the number of layers multiplied by the monolayer thickness.

RESULTS AND DISCUSSION

We have previously demonstrated that LB films represent good model systems for quantitative examination of molecular depth profiling with particular emphasis on the organic−organic interface width.[34] The goal in this work is to optimize the depth resolution in such experiments by investigating the role of various experimental parameters with regard to both the operation of the TOF-SIMS instrumentation and sample preparation. The quality of the depth profile is also determined using parameters evaluated from the previously developed erosion dynamics model.[16]

Single-Component LB Films. Single-component LB films of AA or DMPA are building blocks for alternating LB films and were therefore examined first by C_{60}^+ depth profiling as a reference for later profiles on multilayer structures. The two single-component samples contain 39 layers of AA or 40 layers of DMPA on top of 3 layers of AA, leading to total film thicknesses of 105 (AA) or 96 nm (DMPA), respectively. It is important to note that

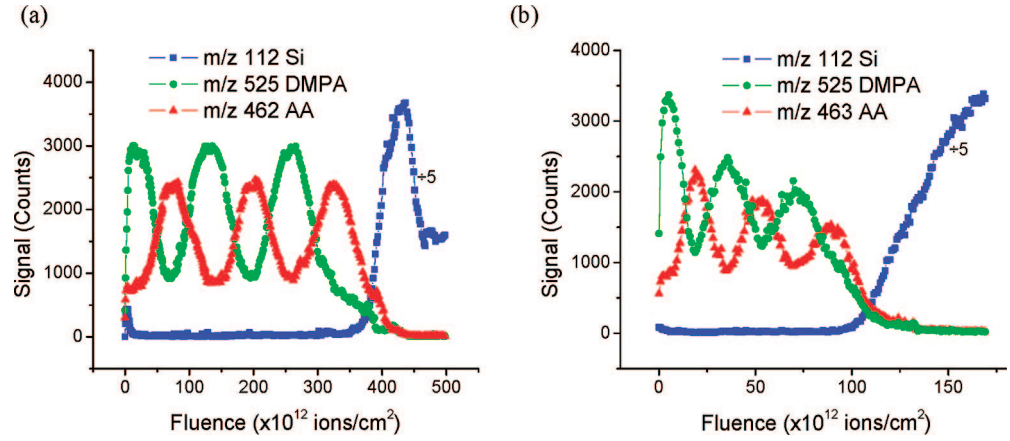

Figure 6. Depth profiles of alternating LB film of DMPA and AA deposited on ozone-treated substrate measured at liquid nitrogen temperature using (a) 20-keV C_{60}^{+} and (b) 80-keV C_{60}^{2+} projectile ions.

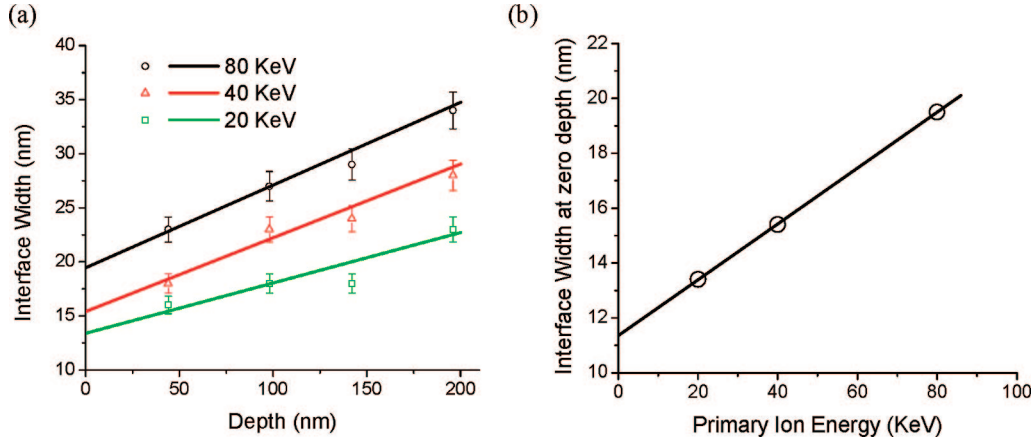

Figure 7. (a) Interface width increment with depth for alternating LB films (ozone-treated substrates) for different primary ion energy, and (b) interface width at zero depth plotted against primary ion energy. The error bars are ±5% of the calculated value.

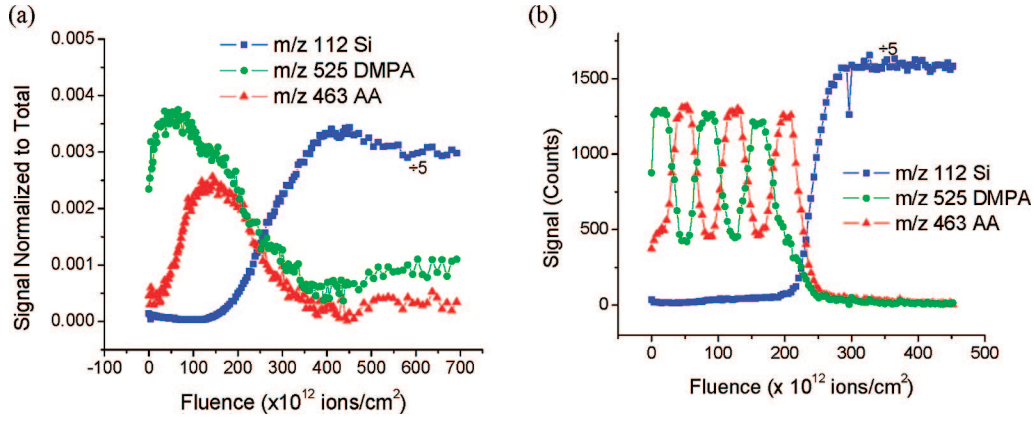

Figure 8. Depth profiles of alternating LB film of DMPA and AA deposited on ozone-treated Si substrate measured at liquid nitrogen temperature using 40-keV C_{60}^{+} projectiles impinging under (a) 5° and (b) 73° with respect to the surface normal.

DMPA multilayers do not form directly on Si but can be built on top of three layers of AA that are first deposited on the Si substrate. Since the DMPA layer is much thicker than the bottom AA layers and the signal of AA is not observed in the depth profile, this sample is still considered to be a single-component film.

Depth profiling was performed both at room temperature (RT) and at cryogenic temperature with the sample stage continuously cooled by liquid nitrogen (LN_2). The resulting profiles are shown in Figure 1. Representative molecular signals of AA and DMPA at m/z 463 and 525, respectively, are plotted together with a substrate signal at m/z 112 for Si_4^{+}. The Si_4^{+} ion signal is used in place of the Si^{+} ion signal since there are fewer isobaric interferences at m/z 112 than at m/z 28. The depth profiles can be divided into three specific regions. At the beginning, the molecular ion signal increases to a maximum and decreases very slightly afterward. This "surface transient" region looks very

similar in all four profiles depicted in Figure 1. The characteristics of the second region, where the bulk of the LB film is being continuously removed, vary as a function of the sample temperature. While the LN_2 profile exhibits a steady state that persists until the film is completely removed, the RT profile exhibits a gradual decline of the molecular ion signal. The third region is characterized by the interface between the organic layer and the Si substrate, where the molecular ion signals decrease rapidly and the Si ion signal emerges.

The initial signal increase appears to be mainly associated with the removal of surface contamination. This interpretation is corroborated by the finding that the initial transient is much less pronounced in depth profiles taken of freshly prepared films and significant changes are observed in the low-mass region of the SIMS spectrum. The behavior is in contrast to the surface transient associated with peptides in trehalose where a much larger increase in the quasi-molecular ion $(M + H)^+$ is observed. This difference might be associated with the observation that C_{60}^+ ion bombardment effectively increases the proton concentration in the near-surface region. Protonation is presumably not involved in the ionization mechanism for the barium salt studied here, hence resulting in different behavior at low fluence.

The small decay of the molecular ion signal immediately after the initial surface transient is of special interest. This decay has been described quantitatively using a simple erosion dynamics model developed previously.[16,21,34] With this model, the signal is predicted to decrease exponentially to a steady-state value due to the building of chemical damage induced by the primary ion beam. In addition, there may be a slower decay of the steady-state signal due to a reduction of the total sputtering yield or erosion rate. Although the cause of this reduction is not known at the moment and no clues are evident in the SIMS spectra, we speculate that it arises from the formation of small carbon particles that eventually agglomerate. It is known that graphitic carbon has a significantly reduced sputtering yield under C_{60}^+ bombardment.

From the erosion dynamics model, the steady-state signal S_{ss} is related to the initial signal S_0 determined by extrapolation to zero fluence as,

$$S_{ss} = S_0 \frac{Y^{tot}}{Y^{tot} + nd\sigma_d} \tag{1}$$

where Y^{tot} is the total sputter yield, σ_d the damage cross section, d the altered layer thickness, and n the molecular number density of the film.[16] The significance of these parameters has been discussed in detail recently.[16] In particular, the magnitude of the exponential decay is connected to a cleanup efficiency parameter ϵ, where

$$\varepsilon = \frac{Y^{tot}}{nd\sigma_d} \tag{2}$$

As is clear from the data in Figure 1, there is virtually no exponential decay in the molecular depth profiles, meaning $Y^{tot} \gg nd\sigma_d$ and ϵ is very large, both at room and at LN_2 temperature. There is, however, a significant slow decay of the signal for the RT samples. Although the mathematical form of $Y^{tot}(f)$ is not known, a slow exponential decay has been found to fit the data for C_{60}^+ bombardment of Irganox films at RT.[22] Since the decay rate is very slow, it can be approximated by a linear relation as

$$Y^{tot}(f) = Y^{tot}(0)[1 - af] \tag{3}$$

where a is a decay cross section related to sputtering. If we assume that the measured molecular ion signal at any given fluence $S(f)$ is proportional to $Y^{tot}(f)$, then

$$S(f) = S_0[1 - af] \tag{4}$$

and a is easily determined from the depth profile. From the data in Figure 1, it is clear that the value of a is nearly zero for the LN_2 samples. It is ~1 nm^2 for AA at RT and ~0.2 nm^2 for DMPA at RT. For Irganox films bombarded by 30-keV C_{60}^+ ions at RT, a value of 0.6 nm^2 is reported[24] (represented as σ_{DS}), in reasonable agreement to the findings reported here.

Multilayer Structures. The next step is to examine the behavior of alternating multilayer LB films. Depth profiles acquired at room and LN_2 temperature are shown in Figure 2 for a film consisting of six building blocks of either AA or DMPA multilayers. Beginning at the surface (top), blocks 1 and 3 each contain 20 layers of DMPA (44 nm), while blocks 2 and 4 consist of 20 layers of AA (54 nm). Blocks 5 and 6 are slightly thicker and consist of 22 layers of DMPA (48 nm) or 23 layers of AA (62 nm), respectively. In both profiles, the molecular ion signal representing the uppermost DMPA block is found to increase after initial ion bombardment, in the same fashion as seen for the single-component films. The apparent AA signal visible at the beginning of the RT profile increases slightly, presumably due to isobaric surface impurities, since the mass spectrum measured in this region is quite different from that measured within an AA block. Upon further irradiation, the two signals continue to alternate in intensity until the Si interface is reached, thus correctly reflecting the chemically alternating structure of the film.

The most significant difference between the two profiles displayed in Figure 2 is the apparent loss of contrast with increasing depth, which is observed in the RT profile but is less pronounced at LN_2 temperature. It is tempting to attribute this finding to a degradation of depth resolution with increasing eroded depth; however, this effect would lead to a symmetric decrease and increase of the signal maximums and minimums, respectively, leaving the average signal largely constant. Instead, the signal maximums observed in Figure 2b decrease a factor of ~2.3 when comparing the beginning block to the final block, while the signal minimums remain virtually unchanged. Hence, we conclude that the apparent loss of contrast in the RT data is mainly attributed to a reduction of the (average) molecular ion signal.

In addition to a decrease in the contrast observed for the RT profile, the erosion rate is observed to decrease with fluence. Assuming the DMPA−AA interface is located at the points where the representative signals match, it is possible to calculate the average sputter yield for each block from the known fluence and block thickness. These yields are reported in Table 1 for both the room and LN_2 temperature depth profiles. Note that the total sputter yield drops by ~30% for the RT sample, but is virtually constant for the LN_2 sample. These yields are plotted in Figure 3 and are seen to decrease nearly linearly with fluence as predicted

by eq 3, using a sputter yield reduction cross section of ~0.14 nm^2. Interestingly, this value is smaller than that determined for the single-component films. It is, however, similar to that determined for cholesterol films[21] under the same bombardment conditions as employed here, indicating that the fluence-dependent sputter yield reduction might be a rather general observation in C_{60} sputter depth profiling.[24]

It is interesting to note that the molecular ion signal drop observed in Figures 1 and 2 is larger than that of the total sputter yield. For instance, the DMPA sputter yield drops to 80 and 71% from the top to the middle and bottom block of the multilayer sample, while the signal maximums drop to 50 and 30%, respectively. A similar trend is observed for the AA films and the AA blocks. This observation is consistent with the erosion dynamics model, which predicts the "quasi-steady-state" signal varies as $(Y^{tot})^{\delta}$ with values of δ between 1 and 2, depending on whether the cleanup efficiency is large ($\delta \sim 1$) or small ($\delta \sim 2$) (see eq 1).

In summary, the RT depth profiles exhibit a drop in yield with fluence that is not observed for the LN_2 temperature experiments. It is not clear why the temperature exerts this effect on the profile, but it is not likely related to any change of the film chemistry, since the mass spectra are essentially the same as those obtained at RT. The LN_2 depth profiles of LB films exhibit less chemical damage. Hence, subsequent studies are performed exclusively under LN_2 conditions.

Surface Topography. The essential step in construction of LB multilayer films is to begin with a well-ordered initial monolayer. A common strategy for preparing the Si substrate is piranha etch, which is effective at removing organic adducts and ensuring hydrophilicity. The etching process, however, leads to enhanced surface roughness. Since the roughness of the resulting LB films might be related to the roughness of the starting Si surface, smoother Si substrates are needed to achieve artifact-free measurements of the depth resolution. Two additional methods were developed to explore the importance of topography on the depth profiles. With one scheme, the Si is exposed to UV ozone for 10 min, and with a second scheme, the Si substrates are sonicated in methanol for 15 min. Both procedures were followed by rinsing with ultrapure water to ensure hydrophilicity. The alternating LB films were then synthesized in the same fashion as described previously. The root-mean-square roughness values measured for Si and the LB films before and during the depth profile analysis are listed in Table 2, and representative AFM images are shown in the Supporting Information. As expected, the methanol-cleaned substrates yield the smoothest LB films and the piranha-etched films exhibit the most topography. The resulting LB films are usually ~10 nm rougher than their original substrates. However, the roughness does not change significantly after C_{60}^+ bombardment at LN_2 temperature for any of the films studied here.

Representative depth profiles for each of these films are shown in Figure 2c and Figure 4. Qualitatively, the three depth profiles are similar in shape as expected. The fluence value needed to reach the Si interface is also about the same for the three profiles, suggesting that sample topography does not change the sputter yield significantly. The difference in signal intensity is due to the use of a different primary ion current during acquisition of the spectra. The profile of the LB film on methanol-treated substrates (Figure 4b) has a relatively lower AA signal compared to that of DMPA, although the signal contrast is still about the same as that in other profiles. The post-interface dip in the Si signal observed in the profile of Figure 4a probably arises from the formation of a silicon oxide layer formed during O_3 treatment of the substrate.

It is possible to estimate the depth resolution of alternating multilayer films utilizing the signal contrast in the measured depth profile.[34] The "interface width", i.e., the full half-width of the (Gaussian) depth response function, determined in this way is plotted against the depth of the interface for all three profiles depicted in Figure 2c and Figure 4. In all three cases, the interface width is found to increase with increasing depth. A linear fit of the data displayed in Figure 5 shows that a rougher sample exhibits a larger increment of the interface width with increasing depth. However, when extrapolated to zero depth, the (virtual) interface width at the beginning of the ion bombardment is ~15 nm in each case. There are many factors that could contribute to the measured interface width. These include: (i) the depth of origin of the sputtered secondary ions, (ii) ion-induced interface mixing effects, and (iii) lateral fluctuations of the LB film thickness. With the latter being of the order of 10 nm—as deduced from the roughness measurements—we estimate 5−10 nm of the zero depth interface width is attributed to the "intrinsic" depth resolution of the method. This finding is consistent with model computer simulations of 20-keV C_{60} bombarding Ag, which indicate the formation of an altered layer thickness of several nanometers.[10,11] Moreover, the depth of origin of Ag^+ ions ejected through a 2.5-nm ice overlayer is estimated to be ~7 nm at 20 keV.[18]

An interesting question remains regarding the cause of the different slopes observed in Figure 5. Apparently, an initially rougher film exhibits a larger degradation of depth resolution with increasing eroded depth. It is tempting to attribute this observation to the development of further, ion bombardment-induced roughness at the bottom of the eroded crater. In fact, topography has been suggested to largely determine the observed depth resolution during the analysis of Irganox3114 δ layers embedded in an Irganox1010 matrix.[25] However, this effect can be excluded here, since the roughness measured after erosion of a significant part of the film is similar to that measured on the original surface. The observed degradation of depth resolution must therefore be induced by an accumulation of ion-induced interface mixing during the removal of the film. Why this should depend on the original roughness of either the substrate surface or the deposited film surface is unclear at the present time.

Primary Ion Energy and Incident Angle Effect. All depth profiling experiments presented so far have been performed with 40-keV C_{60}^+ ions impinging under an incident angle of 40° relative to the surface normal. In this section, the role of projectile impact energy and angle is studied. Note that all results presented below were obtained on alternating LB films built on ozone-treated substrates analyzed at LN_2 temperature.

The depth profiles using 20-, and 40-, and 80-keV C_{60}^{2+} ions for both sputter erosion and data acquisition are shown in Figures 6a, 4a, and 6b, respectively. The ion fluence required to reach the Si interface is $\sim 1 \times 10^{14}$ cm^{-2} at 80 keV, 2×10^{14} cm^{-2} at 40 keV, and 4×10^{14} cm^{-2} at 20 keV. As discussed above, this number is related to the total sputter yield, which is found to increase

linearly with projectile impact energy. This observation agrees with results obtained for C_{60}^+ bombardment of other systems.[28] Comparing the linear slope of the yield versus energy curve by means of the reduced sputter yield volume,[25] Y_{tot}/n, we find the resulting average value of 3.8 nm^3 removed per C_{60} ion and keV of impact energy to agree well with values of 4−8 nm^3/keV measured for trehalose,[36] cholesterol,[21] and Irganox1010 films.[25]

In addition to the difference in sputter yield, the 20-keV depth profile appears to be essentially the same as the 40-keV depth profile, while at 80 keV, the signal maximums gradually decline with increasing ion fluence. At the same time, the fluence needed to remove the individual layers again increases with increasing depth as was found for the RT depth profiles noted above. At 80-keV bombardment, then, there is a fluence-dependent yield reduction even at LN_2 temperature. Apparently, the yield reduction is induced by a thermally activated process that is more likely to occur at higher impact energies.

It is possible that the yield reduction is caused by accumulation of carbon precipitates at the surface of the bombarded film. There is strong experimental[20] and theoretical[37] evidence that a fraction of incident projectile atoms are being implanted into the irradiated surface. In fact, this effect is known to lead to a complete quenching of the sputter yield if Si is bombarded with C_{60} ions of less than 10 keV.[20,38] A similar effect has been observed for Irganox films. The notion is that the deposited carbon atoms form precipitates of an amorphous, graphite-like structure,[20] which is known to have a very low sputter yield.[39,40] Simulations and experiments performed on SiC targets show that single C atoms distributed evenly within a Si crystal do not produce a significant yield reduction.[39] In order to be effective, the implanted carbon atoms need to cluster and eventually form precipitates. At low temperatures, the mobility of the implanted projectile atoms is decreased and the formation of carbon precipitates is hindered, thereby efficiently suppressing the yield reduction. At larger impact energy, on the other hand, more energy is deposited in a single impact, increasing mobility and, hence, counterbalancing the effect of reduced temperature.

The interface width as a function of depth and primary ion kinetic energy are shown in Figure 7a. For all three impact energies, the interface width scales linearly with depth with a slightly different slope. The zero depth interface width as a function of the primary ion energy is shown in Figure 7b. Lower impact energy clearly leads to better depth resolution, a finding that is well-known for inorganic systems.[41] This effect is understandable since the zero depth interface width depends upon the altered layer thickness, which increases with increasing energy. By extrapolating to zero impact energy, a virtual interface width is obtained, which should to first order be stripped of bombardment-induced effects. In principle, this value should be solely determined by the information depth of the (static) method applied to analyze the surface chemistry. The reported value of ~11.5 nm, however, appears to reflect mainly the fluctuations of film thickness (about 10 nm, see above). More detailed artifact-free measurements of this parameter will be increasingly difficult since it appears to approach a value of just a few nanameters.

The effect of incident angle on the depth resolution is quite dramatic. The representative depth profiles of the alternating LB films using 40-keV C_{60}^+ at near-normal incidence (5° relative to surface normal) and glancing angle (73° relative to surface normal) are displayed in Figure 8. The comparable profile at 40° incidence is displayed in Figure 4a. Under glancing incidence, the profile looks similar to that at 40° incidence, as shown in Figure 8b. However, the depth resolution appears to be slightly improved, since the observed signal maximums reach an observable steady state at the center of each block. On the other hand, the result obtained under normal incidence is catastrophic as shown in Figure 8a. The profile barely resolves the alternating chemical structures except that the DMPA signal drops slightly while the AA signal increases from baseline at the first DMPA−AA interface. This result implies that the depth resolution is even larger than the thickness of the chemical block (44 nm for DMPA and 54 nm for AA). Molecular dynamics simulations have shown that the energy of the primary ion is deposited much deeper under normal incidence conditions than oblique impact angles.[42] At the same time, the altered layer thickness is experimentally measured to be larger as well.[21] Apparently, both effects combine to effectively worsen the achievable depth resolution. At glancing impact angle, on the other hand, the primary ions are more like "peeling" off the surface layer, leaving the molecules underneath better preserved. Compared to 40° incidence, however, the enhancement at glancing angle is not as dramatic as the reduction at normal incidence, a finding that also agrees with computer simulations.[42]

CONCLUSIONS

Using multilayer LB films as a model for molecular depth profiling, various experimental parameters were investigated for their effects on the quality of depth profiling. The results show that profiles with relatively stable signal maximums and uniform sputter yield are achieved by lowering the sample temperature to cryogenic condition. The depth resolution is found to deteriorate slightly with increasing primary ion fluence, an effect that does not appear to be directly related to increasing ion-induced roughness. The parameters of the primary ion beam also play an important role in optimizing the molecular depth profiling experiment. The depth resolution is found to be improved at lower C_{60}^+ kinetic energy, the zero depth interface width scaling linearly with impact energy. If extrapolated to zero impact energy, we find a virtual interface width that is to a large extent determined by fluctuations of the LB film thickness, leaving only a few nanameters as the physical limit of the achievable depth resolution. Variation of the projectile impact angle reveals that the depth resolution is slightly enhanced under glancing incidence (compared to 40° impact), while the quality of the depth profile is much worse under normal incidence. These observations agree with the predictions of molecular dynamics computer simulations. In summary, we suggest use of the lowest possible impact energy, which is compatible with good beam focusing conditions needed for high-resolution three-dimensional imaging applications—and

(36) Wucher, A.; Cheng, J.; Winograd, N. Appl. Surf. Sci. In press.
(37) Krantzman, K. D.; Kingsbury, D. B.; Garrison, B. J. *Appl. Surf. Sci.* **2006**, *252*, 6463–5.
(38) Fisher, G. L.; Dickinson, M.; Bryan, S. R.; Moulder, J. *Appl. Surf. Sci.* In press.
(39) Krantzman, K. D.; Webb, R.; Garrison, B. J. *Appl. Surf. Sci.* In press.
(40) Kozole, J., Wuche, A., Winograd, N. Unpublished data.
(41) Hofmann, S. *Philos. Trans. R. Soc. London, Ser. A* **2004**, *362*, 55–75.
(42) Ryan, K. E.; Garrison, B. J. *Appl. Surf. Sci.* In press.

glancing incidence in combination with low sample temperature to achieve optimum depth resolution in molecular depth profiling experiments.

ACKNOWLEDGMENT

Financial support from the National Institute of Health under grants EB002016-13 and GM069338, the National Science Foundation under grant CHE-0555314, and the Department of Energy grant DE-FG02-06ER15803 are acknowledged. The authors also thank Prof. David L. Allara and his research group for the use of ellipsometry equipment, and Dr. Joesph Kozole for building the special sample holder for incident angle experiments.

SUPPORTING INFORMATION AVAILABLE

Representative AFM images of sample roughness (Figure S1). This is material is available free of charge via the Internet at http://pubs.acs.org.

Received for review May 23, 2008. Accepted July 30, 2008.

AC801056F